SCIENCE CHINA
Earth Sciences

•ARTICLE•

July 2024 Vol.67 No.7: 2242–2252
https://doi.org/10.1007/s11430-024-1346-2

Productivity in the Southern Ocean Antarctic Zone during the Northern Hemisphere Glaciation (NHG) and its link to atmospheric pCO_2

Yiming WU[1], Jingteng GUO[1,2], Xiangyu ZHAO[3,4], Wenshen XIAO[5], Heng LIU[1], Zhifang XIONG[1,2*] & Tiegang LI[1,2*]

[1] *Key Laboratory of Marine Geology and Metallogeny, First Institute of Oceanography, Ministry of Natural Resources, Qingdao 266061, China;*
[2] *Laboratory for Marine Geology, Laoshan Laboratory, Qingdao 266237, China;*
[3] *School of Oceanography, Shanghai Jiao Tong University, Shanghai 200030, China;*
[4] *Key Laboratory of Polar Ecosystem and Climate Change, Shanghai Jiao Tong University, Ministry of Education, Shanghai 200030, China;*
[5] *State Key Laboratory of Marine Geology, Tongji University, Shanghai 200092, China*

Received January 23, 2024; revised May 20, 2024; accepted May 23, 2024; published online June 12, 2024

Abstract A decrease in atmospheric CO_2 partial pressure (pCO_2) is considered an important prerequisite for the onset and intensification of Northern Hemisphere Glaciation (NHG). However, how the ocean sequestered missing CO_2 during the NHG is still uncertain. Changes in surface productivity and deep ventilation in the Southern Ocean (SO) have been proposed to explain the variations in atmospheric pCO_2 over the last eight glacial cycles, but it is unclear whether these mechanisms contributed to the decrease in atmospheric pCO_2 during the NHG. Using titanium-normalized contents and mass accumulation rates of biogenic opal and total organic carbon from the International Ocean Discovery Program (IODP) Expedition 374 Site U1524A, we reconstruct the productivity in the Ross Sea, Antarctica, from 3.3 Ma to 2.4 Ma. The productivity records exhibit a long-term decreasing trend and several distinct phased evolutionary features. Specifically, the local productivity fluctuated dramatically during 3.3–3.0 Ma, decreased gradually during 3.0–2.6 Ma, and remained relatively constant during 2.6–2.4 Ma. By comparing productivity with its potential influences, we infer that the phased and long-term evolutions of productivity were mainly controlled by changes in deep ocean ventilation. Sea ice expansion might have decreased productivity during 3.3–3.0 Ma by light attenuation. Changes in eolian dust input have little effect on productivity. Further analysis revealed no coupling linkage between productivity and atmospheric pCO_2, indicating that the productivity in the SO Antarctic Zone (AZ) was not the main factor controlling the atmospheric CO_2 decrease during the NHG. To improve our understanding of the role of SO processes in the NHG, further studies should focus on the potential influences of deep ocean ventilation on atmospheric pCO_2 in the AZ, and similar studies should also be extended to the sea area in the Subantarctic Zone.

Keywords Ross Sea, Biogenic opal, Total organic carbon, Deep ocean ventilation, Sea ice, Ocean carbon cycle

Citation: Wu Y, Guo J, Zhao X, Xiao W, Liu H, Xiong Z, Li T. 2024. Productivity in the Southern Ocean Antarctic Zone during the Northern Hemisphere Glaciation (NHG) and its link to atmospheric pCO_2. Science China Earth Sciences, 67(7): 2242–2252, https://doi.org/10.1007/s11430-024-1346-2

* Corresponding authors: Zhifang XIONG (zhfxiong@fio.org.cn), Tiegang LI (tgli@fio.org.cn)

1. Introduction

The Pliocene-Pleistocene climate transition was a major transition in the global climate, which represented an important transition from the persistent warmth of the middle to late Pliocene to the cyclic glaciations of the Quaternary. During the Pliocene warm period (4.5–3 Ma), the Earth′s surface temperature was ~3°C higher than that at present, the atmospheric pCO_2 was as high as ~400 ppmv (1 ppmv= 1 μL L^{-1}) compared to 172–300 ppmv during the late Quaternary, and the meridional sea surface temperature gradient was relatively small (Haywood and Valdes, 2004; Lüthi et al., 2008; Brierley et al., 2009; Seki et al., 2010). During this period, the West Antarctic ice sheet partially retreated, and the Arctic Ocean was still almost ice free (Naish et al., 2009; Ballantyne et al., 2010, 2013). Global cooling intensified abruptly in the late Pliocene (~2.75 Ma), characterized by an intensified glaciation, a significant increase in the Northern Hemisphere ice volume, and periodical expansion and retreat of the Northern Hemisphere ice sheet (Mudelsee and Raymo, 2005; Blake-Mizen et al., 2019). The global climate entered the Quaternary epoch, with fluctuations in response to the 41-kyr obliquity forcing (Lisiecki and Raymo, 2005), and the Northern Hemisphere Glaciation (NHG) initiated. The NHG amplified, synchronized and even drove global climate change on different time scales through the interaction of the expanding ice sheet with other climate system components (Clark et al., 1999).

Numerous hypotheses have been proposed to explain the NHG. These include the uplift of the Tibetan Plateau, the deepening of the Bering Strait or the Greenland-Scotland Ridge, the restriction of the Indonesian seaway, and the closure of the Panama seaway (Ruddiman et al., 1986; Raymo, 1994; Wright and Miller, 1996; Cane and Molnar, 2001; O'Dea et al., 2016). These tectonic events could alter the meridional heat and moisture transfer to the Northern Hemisphere and thus contribute to the NHG. However, due to the imprecise definition on dating and magnitude of these tectonic activities, as well as their chronological discrepancies from the NHG, it is evident that these hypotheses alone cannot explain the origin of the NHG (Raymo, 1994; Willeit et al., 2015; Jaramillo et al., 2017). A decrease in atmospheric pCO_2 is another possible mechanism driving the NHG (Willeit et al., 2015). And the pCO_2 threshold value of 280 ppmv for the initiation of the NHG has been confirmed by several simulations and paleoceanographic results (Seki et al., 2010; Martínez-Botí et al., 2015; Stap et al., 2016). The atmospheric pCO_2 decrease would further amplify NHG climate cooling (DeConto et al., 2008). To date, existing studies have predominantly focused on the role of high-latitude heat transport in NHG initiation from the "oceanic tunnel" perspective, while less studies have explored the sequestration of missing atmospheric pCO_2 during the NHG from the "atmospheric bridge" perspective. For example, McKay et al. (2012) suggested that Southern Hemisphere cooling during 3.3–2.5 Ma affected oceanic teleconnection and thus weakened the Atlantic Meridional Overturning Current (AMOC), which reduced northward heat transport and contributed to NHG initiation. Woodard et al. (2014) suggested that the Antarctic ice sheet expansion during 3.2–2.7 Ma enhanced the stratification of the Southern Ocean (SO), allowing warm water that would have upwelled in the North Atlantic via the AMOC to submerge deeper into the Pacific Ocean. These studies have disregarded the role of atmospheric pCO_2 during the NHG, which is the scientific concern of the present study.

The SO regulates global climate change on both modern and orbital time scales by sequestering and releasing carbon through local biological, physical, and chemical processes. Approximately 40% of anthropogenic CO_2 sequestration in the oceans occurs in the SO (Khatiwala et al., 2009). The SO can absorb atmospheric CO_2 through photosynthesis by plankton in surface water and can also release "respired CO_2" from the ocean interior to the atmosphere. The carbon budget of these two processes determines whether the SO is storing carbon, which ultimately influences atmospheric pCO_2 (Watson and Garabato, 2006; Fischer et al., 2010; Watson et al., 2015). Some studies suggest that glacial-interglacial variations in atmospheric pCO_2 can be driven by SO processes alone. Specifically, enhanced glacial stratification in the Antarctic Zone (AZ) not only reduces local productivity but also decreases the release of CO_2 from the ocean to the atmosphere by decreased ocean ventilation. In the Subantarctic Zone (SAZ), the glacial increase in phytoplankton production driven by increased eolian dust input allows more atmospheric CO_2 to be sequestered in the ocean. Taken together, these processes have contributed to the decrease in atmospheric pCO_2 during glaciations (Jaccard et al., 2013; Martínez-García et al., 2014). These mechanisms may account for the linkages between SO productivity, ocean ventilation, and atmospheric pCO_2 over the past 800 kyr. However, it remains unknown whether these scenarios could be applicable on longer time scales. Therefore, reconstructing SO productivity and testing its linkage with atmospheric pCO_2 during the NHG are important for revealing the driving mechanism for the NHG.

In this study, using biogenic opal and total organic carbon (TOC) content data from Site U1524A, which was drilled during the International Ocean Discovery Program (IODP) Expedition 374 in the Ross Sea, Antarctica, we reconstructed the productivity during 3.3–2.4 Ma. Then, we revealed the factors controlling the productivity and discussed the linkage between productivity and atmospheric pCO_2, to provide insights into the mechanism of the NHG.

2. Regional setting

The Ross Sea is located in the Southwest Pacific sector of the SO (170°E–140°W), with Mary Bird Land and Victoria Land as its eastern and western boundaries, respectively. The southern boundary of the Ross Sea is connected to the Ross Ice Shelf (RIS), which is the largest ice shelf in the world. The Ross Sea is the second largest marginal sea in the SO (Figure 1a, 1b). The modern Ross Sea is strongly affected by seasonal sea ice, with winter sea ice coverage extending up to approximately 60°S off the outer marginal sea. In summer, the melting of the RIS could decrease the sea ice coverage to 20% of the extent in winter (Massom and Stammerjohn, 2010; Liu et al., 2016). The Ross Sea is a region with high nutrient and chlorophyll levels and is one of the most productive regions in the SO, with nutrient-enriched surface waters during the productive season (Arrigo et al., 2008; Smith et al., 2012).

Warm and nutrient-rich Circumpolar Deep Water (CDW) is widely distributed in the SO and is important for local productivity. CDW can feed into Antarctic Bottom Water (AABW) at the edge of the outer continental shelf (Figure 1b). CDW upwells in the Ross Sea and mixes with other water masses to form Modified Circumpolar Deep Water (MCDW). MCDW is less saline, warmer and nutrient-rich, and can promote productivity on the Ross Sea shelf and upper continental slope (Smith et al., 2012; Figure 1c). When the RIS expands or sea ice coverage increases, high-salinity shelf water (HSSW) with a low temperature and high density forms in the surface ocean. HSSW formation leads to vertical water column stratification. Due to its high density, the northward-flowing HSSW feeds into the AABW at the continental slope (Basak et al., 2015; Figure 1b). The ice shelf water (ISW) produced by melting glaciers is characterized by low temperature, salinity and density, and it also feeds into the AABW at the continental shelf break (Figure 1b). The AABW, which converges from the outer shelf edge to the southern edge of the southeast Pacific basin, is characterized by low temperature and high salinity (Gordon et al., 2004) and plays an important role in the global thermohaline circulation. The Ross Sea, a major area of AABW production, contributes approximately 25% of the AABW (Orsi et al., 2002). The Antarctic Slope Current (ASC), which surrounds the Antarctic continent, is widely distributed in the subsurface of the SO and plays an important role in regulating the upwelling of CDW to the Ross Sea shelf (Thompson et al., 2018).

3. Materials and methods

3.1 Site U1524A

Site U1524A, which was drilled in the Ross Sea during IODP Expedition 374 in 2018, is located ~120 km north of the Ross Sea continental shelf edge on the eastern levee of the Hillary Canyon at a water depth of 2394.39 m (Figure 1c). Hole U1524A was drilled to a depth of 299.5 m CSF-A and obtained a core length of 282.35 m CSF-A, with an overall percentage of core recovery of 94.27%. Based on the shipboard core description, Site U1524 could be divided into three stratigraphic units according to diatom abundance. Hole U1524A contains the whole of unit I (200.55–0 m CSF-A) and the majority of unit II (290.36–200.55 m CSF-A). Unit I is characterized by layers of diatom ooze and diatom-rich mud, and Unit II is characterized by diatom-rich sandy mud and muddy diatom ooze. Unit I can be further subdivided into three subunits: subunit IA (78.03–0 m CSF-A), consisting of diatom-bearing mud and diatom-rich mud; subunit IB (155.58–78.03 m CSF-A), consisting of diatom-rich mud/sandy mud and diatom ooze; and subunit IC (200.55–155.58 m CSF-A), consisting of diatom-rich mud and muddy diatom ooze. This study used the 270–78 m CSF-A of the hole, with a sampling interval of 0.2 m for the 120–78 m CSF-A and a sampling interval of 0.5 m for the 270–120 m CSF-A. A total of 505 samples were obtained.

3.2 Geochemical analysis

The biogenic silicon (BSi) content was analyzed at the Key Lab of Submarine Geosciences and Prospecting Techniques, Ocean University of China. The BSi was first extracted by wet alkaline extraction and then measured by molybdate blue spectrophotometry (DeMaster, 1981; Müller and Schneider, 1993). Each sample was lyophilized and ground to a size less than 74 μm. Then, 130–140 mg of sample was placed in 5 mL of 10% H_2O_2 to remove the organic matter. After mixing and resting for half an hour, 5 mL of HCl at a volume ratio of 1:9 was added to remove carbonate. After mixing and resting for half an hour, 40 mL of distilled water was added to the treated sample. Then, each sample was centrifuged at 3000 rpm for 10 minutes and dried after removal of the supernatant. Then, 40 mL of 2 mol L^{-1} Na_2CO_3 solution was added to the dried sample. After sufficient mixing, each sample was heated in a water bath at 85 °C for 2 hours. Then, 3 mL of ammonium molybdate was added to 0.125 mL of supernatant from the centrifuged sample. After standing for 10 minutes, 15 mL of reducing agent was added. After 3 hours, the absorbance value of the extract was determined, and the mass fraction of BSi was calculated. The above procedures were repeated six times. The extraction time and the mass fraction of BSi in the extract were used as the horizontal and vertical coordinates, respectively, to derive a linear regression equation for the change in the mass fraction of BSi with time, and its intercept is the BSi content of the sample. The sedimentary biogenetic opal (SiO_2•$0.4H_2O$) content was calculated according to the formula given by Mortlock and

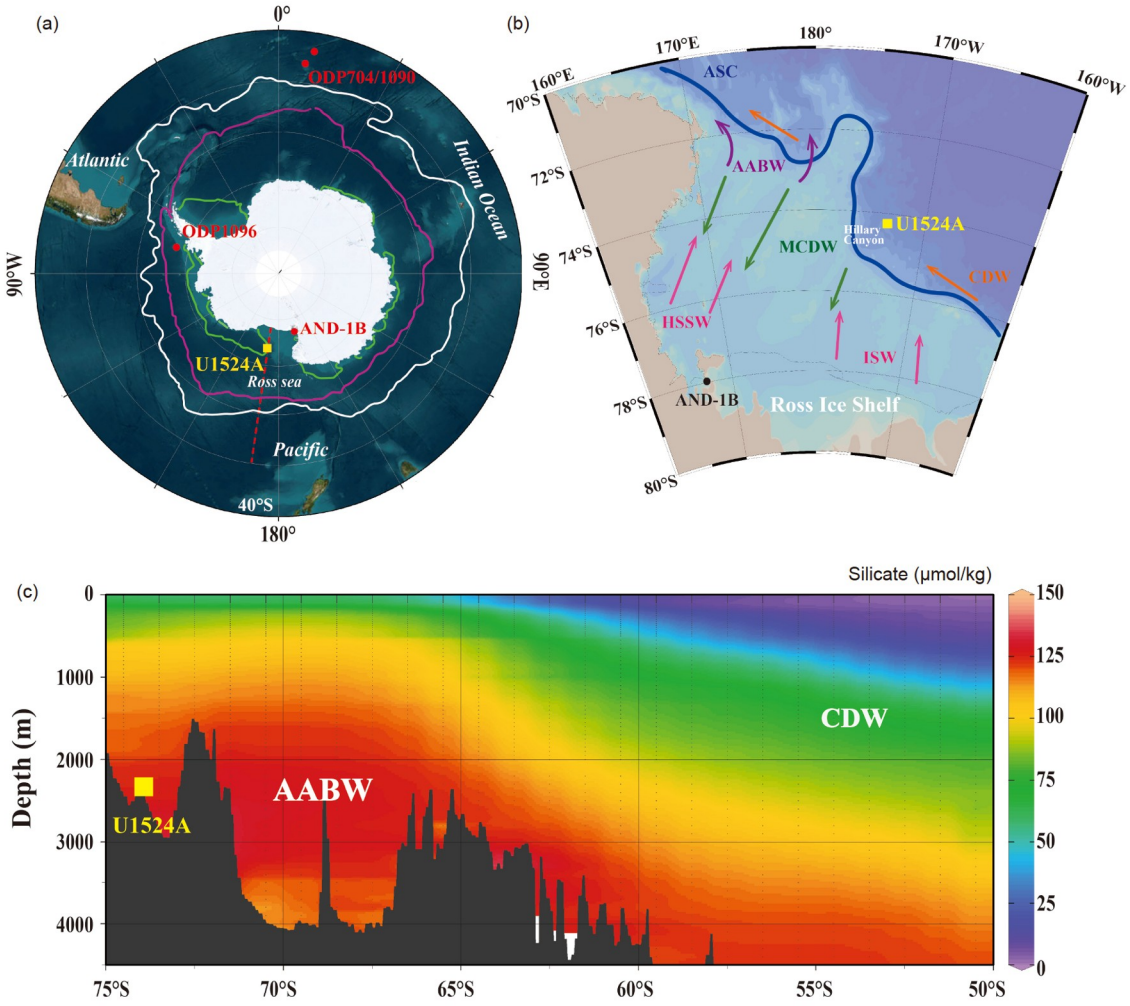

Figure 1 Location of Site U1524A in the Ross Sea. (a) Locations of Site U1524A (this study, yellow square) and other sites (AND-1B (McKay et al., 2012), ODP Site 1096 (Hillenbrand and Cortese, 2006), ODP Site 704 (Hodell and Venz, 1992), and ODP Site 1090 (Venz and Hodell, 2002); red circles) mentioned in the discussion. The white solid line is the modern Antarctic polar front (Trathan et al., 2000). The solid green and pink lines represent the modern summer and winter sea ice coverage, respectively (Fetterer et al., 2017). The red dashed line shows the transect of the silicate concentration in (c). (b) Major currents and water masses in the Ross Sea (pink indicates HSSW/ISW, green indicates MCDW, purple indicates AABW, orange indicates CDW, and blue indicates ASC). (c) Longitudinal bathymetric profile of nitrate concentration in the Ross Sea at 175°W. The map in panel a was created by ArcGIS software, and the maps in panels (b) and (c) were created by Ocean Data View (ODV) software.

Froelich (1989) (opal%=2.4×BSi%). The long-term precision (RSD) of this analytical method was better than ±3%.

The TOC analysis was carried out at the Institute of Oceanology, Chinese Academy of Sciences. Approximately 0.3–0.4 g of the lyophilized sample was weighed and placed into a clean glass vial. Two milliliters of 1 mol L^{-1} HCl was slowly added to remove carbonate, after which the sample was shaken every 8 h to fully remove the inorganic carbon and then rinsed with ultrapure water 5 times after 48 h to remove the chemical residue. The processed samples were dried on a freeze dryer, weighed and ground in preparation for testing. Approximately 30 mg of the sample was accurately weighed, placed in a clean tin cup, packed and compacted, and then placed into a Thermo EA1112 Elemental Analyzer with an autosampler for analysis. Based on the repeatability measurements of calibrated mixing soil standards ($C_{AR4021+IVA99995}$%=1.86%), the analytical precision (RSD) of the method was better than ±1.3%.

Titanium (Ti) and other elemental contents were analyzed at the State Key Laboratory of Geological Processes and Mineral Resources, China University of Geosciences, Wuhan, China. Approximately 50 mg of each sample was weighed in a Teflon vessel, and 1.5 mL HNO_3 and 1.5 mL HF were added to the vessel and then placed in an oven at ~190 °C for 48 h to perform high-temperature and high-pressure digestion. The digested solution was evaporated to dryness, dissolved in 3 mL of the mixed acid (1 mL HNO_3, 1 mL H_2O, and 1 mL 1 ppm In), and then placed into an oven at 190 °C for 12 h for secondary digestion. Finally, the residue was diluted with 2% HNO_3 to the appropriate concentration and subjected to inductively coupled plasma-mass spectrometry (ICP-MS). International rock standards (BCR-2,

BHVO-2, AGV-2 and GSP-2) from the United States Geological Survey were used for pretreatment and on-board testing. The relative errors between the recommended and the measured values of the standard samples were within ±10%. The repeat measurements of the samples showed that the analytical precision (RSD) was within ±5% for most of the elements, including Ti.

3.3 Calculations on Ti-normalized contents and MARs of biogenic components

The Ross Sea is a marginal sea surrounding the Antarctic continent. Terrigenous materials may have a dilution effect on biogenic components, such as opal and TOC. To avoid this effect, Ti, which exhibits conservative geochemical behavior during rock weathering and a very low content in seawater, was selected to normalize the biogenic components (Figure 2b, 2c).

Due to the heterogeneity of compaction degree and moisture content during deposition, the mass accumulation rate (*MAR*) of the biogenic component was calculated to reduce the compaction effect (Rea and Janecek, 1981):

$$MAR_{opal}=\omega_{opal}\times\rho_{dry}\times v, \quad (1)$$

$$MAR_{TOC}=\omega_{TOC}\times\rho_{dry}\times v, \quad (2)$$

where MAR_{opal} and MAR_{TOC} represent the *MAR*s of opal and TOC, respectively; ω_{opal} and ω_{TOC} represent the contents of opal and TOC, respectively; ρ_{dry} represents the dry bulk density (DBD); and v represents the linear sedimentation rate (LSR). To obtain the DBD of each sample used in this study, the high-resolution shipboard gamma ray attenuation data were linearly interpolated to the corresponding sampling strata. Then, the DBD was calculated by using the following linear relationship fitted to the shipboard DBD and the shipboard wet sample density (ρ_{wet}) (R^2=0.97) (Figure 2g):

$$\rho_{dry}=1.436\times\rho_{wet}-1.33. \quad (3)$$

4. Results

4.1 Age model

Due to the lack of foraminifera at Site U1524A, which is located in the high-latitude zone of the SO, the age model can not be established by oxygen isotope testing. Shipboard data show that a total of 12 stratigraphic magnetic inversion events have been identified in the 280–0 m CSF-A interval (McKay et al., 2019), with the oldest magnetic reversal being the *Mammoth*/*Subchrons* boundary (C2An.2r [3.207–3.330 Ma]). A total of 20 biostratigraphic events, involving diatoms and radiolarians, were also identified. Age model for Site U1524A was established by linear interpolation using a combination of absolute ages revealed by shipboard magnetostratigraphic inversion events, shore-based magnetostratigraphic inversion events and shipboard biostratigraphic events (Zhao X, personal communication). Based on this age model, the chronological span of the 270–78 m CSF-A interval of U1524A is 3.3–2.4 Ma (Figure 2). The LSR for this period is generally constant, except for a brief and significant decrease at approximately 3.2–3.1 Ma (Figure 2f), with a range of 12.94 to 25.30 cm kyr^{-1} and a mean value of 20.80 cm kyr^{-1} (Zhao X, personal communication).

4.2 Content of the biogenic component

The opal content at Site U1524A shows a long-term decreasing trend during 3.3–2.4 Ma (Figure 2a). It can be divided into three stages: (1) during 3.3–3.0 Ma, the opal content shows a peak, with a range of variation of 16.85%–50.17% and a mean value of 32.70%; (2) during 3–2.6 Ma, the opal content decreases gradually, with a range of variation of 7.53%–38.77% and a mean value of 25.72%; and (3) during 2.6–2.4 Ma, the opal content remains stable, with a range of variation of 5.02%–32.23% and a mean value of 16.70%. The TOC content shows the same trend as that of opal (Figure 2a). During 3.3–3.0 Ma, the TOC contents vary from 0.10%–0.78%, with a mean value of 0.52%. During 3.0–2.6 Ma, the TOC contents vary from 0.10% to 0.46%, with a mean value of 0.42%. During 2.6–2.4 Ma, the TOC contents vary from 0.07% to 0.57%, with a mean value of 0.39%. The Ti content shows a long-term increasing trend from 3.3 to 2.4 Ma and can also be divided into three stages similar to those of the opal and TOC records (Figure 2b).

5. Discussion

5.1 Productivity variations in the Antarctic Zone

SO sediments are major global sinks for BSi, representing the production, export and deposition of diatoms and other siliceous phytoplankton. The opal content in sediments is mainly controlled by the production of opal in surface water and dissolution in deep waters and on the seafloor. In addition, dilution and compaction could also impact the opal content. The Ti-normalized opal content (opal/Ti) at Site U1524A perfectly agrees with the the opal content record (Figure 2a, 2c), indicating a weak dilution effect of terrigenous components. To date, there is no record of deep silicic acid saturation (or concentration) in the Antarctic Ross Sea during 3.3–2.4 Ma. Given the high burial efficiency and the high rain rate of BSi production in the SO, it is suggested that the content of BSi preserved in the sediments should primarily reflect production rather than dissolution (Pondaven et al., 2000). The TOC content in the SO sediments is mainly controlled by the production of organic carbon by phytoplankton such as diatoms, and their degradation in the water column and pore water. Although the factors affecting TOC degradation differ from those affecting opal dissolution, the

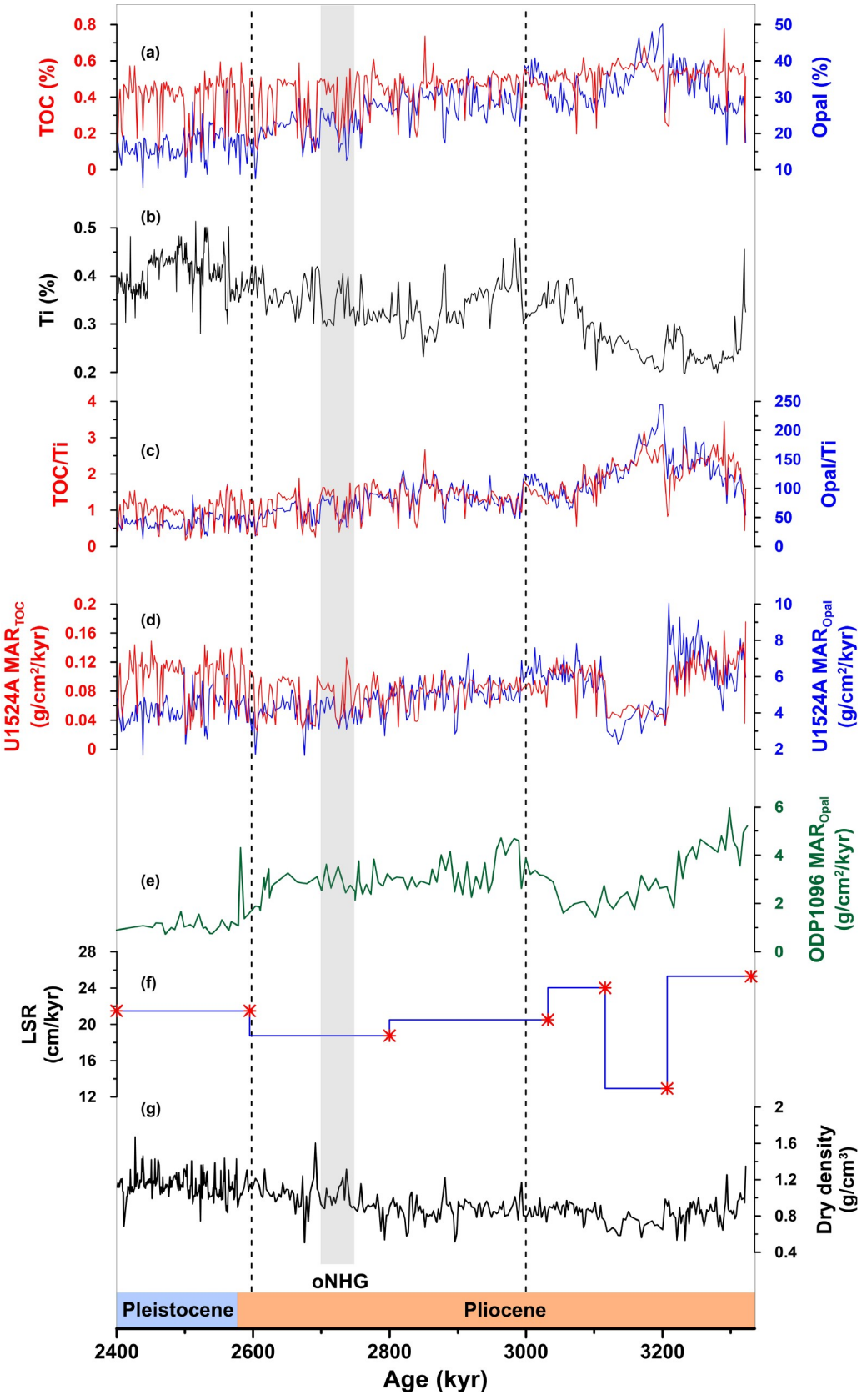

Figure 2 Productivity variations at Site U1524A in the Ross Sea during the NHG. (a)–(d) opal, TOC, Ti contents, opal/Ti, TOC/Ti, MAR_{opal} and MAR_{TOC} at Site U1524A. (e) MAR_{opal} at ODP Site 1096 (Hillenbrand and Cortese, 2006). (f), (g) LSRs, age control points (red stars) (Zhao X, personal communication) and DBDs at Site U1524A. The vertical dashed lines mark the three stages of the productivity evolution, and gray shading indicates the oNHG.

observed trends of the opal and TOC contents, and opal/Ti and TOC/Ti are consistent, respectively (Figure 2a, 2c), further supporting the contention that the opal and TOC contents at Site U1524A are mainly controlled by productivity.

Except for the 3.2–3.1 Ma time interval, opal/Ti and MAR_{opal}, and TOC/Ti and MAR_{TOC} at Site U1524A show consistency respectively, both in terms of detailed and long-term evolution (Figure 2c, 2d). The LSR significantly decreased during 3.2–3.1 Ma, while the DBD changed only slightly (Figure 2g), indicating that the difference between the Ti-normalized biogenic content and the biogenic MAR during 3.2–3.1 Ma was caused by a significantly reduced LSR (Figure 2f). It seems that compaction has had an impact on the accumulation of opal and organic matter during this time interval. Based on the entire record, MAR_{opal} and MAR_{TOC} are more reliable proxies for productivity at site U1524A than opal/Ti and TOC/Ti. Moreover, the MAR_{opal} record at ODP site 1096, which is also in west Antarctica (Hillenbrand and Cortese, 2006), is generally consistent with our MAR_{opal} record (Figure 2d, 2e), supporting the use of MAR_{opal} as a more reliable proxy for productivity. According to the MAR_{opal} and MAR_{TOC} results at Site U1524A, the productivity in the Southern Ocean Antarctic Zone shows a long-term decreasing trend, which can be divided into three stages (Figure 2): (1) the 3.3–3.0 Ma time interval is characterized by dramatic fluctuations in productivity, which shows a trend of increasing, then significantly decreasing, and finally increasing again; (2) the 3–2.6 Ma time interval is characterized by a gradual decrease in productivity; and (3) the 2.6–2.4 Ma time interval is characterized by relatively constant productivity. In particular, during the onset of the NHG (oNHG) at ~2.7 Ma, the productivity reveal no significant change.

5.2 Potential controls on productivity variations in the Antarctic Zone

Productivity in the SO is directly controlled by the availability of surface water nutrients and light conditions. Nutrient availability in surface water mainly depends on ocean ventilation and eolian dust input. Strong ocean ventilation in the SO allows for greater upwelling of deeper nutrients to the surface (Haug et al., 1999; Sigman et al., 2004), and thus, high productivity tends to occur in well-ventilated regions, such as upwelling areas near shelf breaks, polynya systems, and frontal zones (Comiso et al., 1993; Moore and Abbott, 2000; Arrigo and van Dijken, 2003). Eolian dust can provide silicon and iron nutrients that promote or stimulate the growth of phytoplankton such as diatoms, which in turn has an impact on productivity (Boyd, 2002; Martínez-García et al., 2014). Light conditions in surface water mainly depend on the sea ice intensity (i.e., extent and duration of sea ice coverage) and solar radiation intensity. Increased sea ice intensity would reduce the amount of solar radiation received at sea surface, thereby decreasing local productivity (Hall, 2004). In the following, the productivity at Site U1524A is compared with the environmental factors mentioned above to identify the controls on productivity in the AZ at different time scales.

5.2.1 Factors controlling the staged evolution of productivity

The productivity at Site U1524A exhibited a pattern of dramatic fluctuations from 3.3 to 3.0 Ma, characterized by an increasing-decreasing-increasing trend (Figure 3b). Only the deep ocean ventilation indicated by benthic foraminiferal $\delta^{13}C$ records in the SO is consistent with our productivity records (Hodell and Venz, 1992, Hodell and Venz, 2006; Venz and Hodell, 2002) (Figure 3d). Enhanced deep ocean ventilation corresponded to increased productivity, suggesting that nutrients in the deep sea reach the surface through upwelling, increasing nutrient availability and thus productivity. During this period, the eolian dust supply remained relatively low (Martínez-Garcia et al., 2011) (Figure 3d), mainly due to the increase in forest coverage and the continuous contraction of deserts during the mid-Pliocene warm period (Salzmann et al., 2008). Therefore, eolian dust input should not have a significant impact on our productivity results. Diatom assemblages and ice algal content records from AND-1B indicate that the offshore summer sea ice intensity in the Ross Sea began to increase at 3.2 Ma, after which it exploded and persisted by 3.03 Ma (McKay et al., 2012; Riesselman and Dunbar, 2013). Importantly, these discontinuous records provide a rough indication of sea ice enhancement in the Ross Sea since 3.2 Ma, which appears to correspond to the low productivity at 3.2–3.1 Ma (Figure 3e). The strengthening of sea ice intensity from 3.2 Ma onward and the low variability in solar radiation during this period combined to reduce light conditions (Figure 3e, 3f), resulting in a shorter phytoplankton production season, which may have reduced the productivity at 3.2–3.1 Ma (Figure 3b). Taken together, these results suggest that deep ocean ventilation dominated the productivity during 3.3–3.0 Ma, but sea ice may also have had some influence.

The productivity at Site U1524A gradually decreased from 3.0 Ma to 2.6 Ma and did not show dramatic variations similar to those from 3.3 Ma to 3.0 Ma (Figure 3b). During this period, deep ocean ventilation gradually weakened (Figure 3c), while the eolian dust input first remained stable and then slowly increased (Figure 3d), indicating that deep ocean ventilation, rather than eolian dust input, controlled productivity during this period. Because of the lack of an overall trend in insolation from 3.3 Ma to 2.4 Ma (Figure 3f), light conditions were mainly controlled by sea ice intensity. The record of diatom-based sea ice intensity is incomplete for this

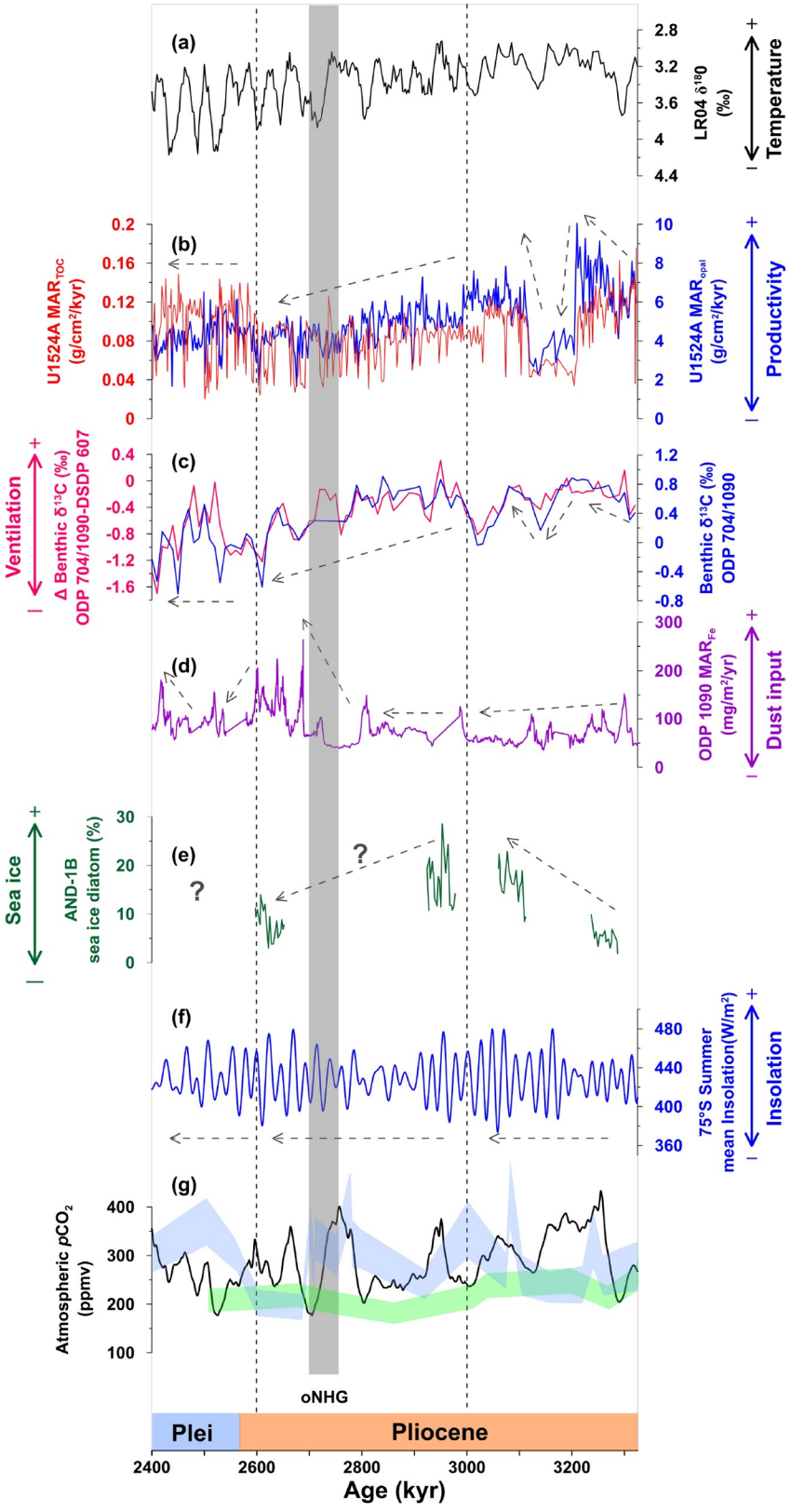

Figure 3 Factors influencing productivity in the Ross Sea. (a) LR04 $\delta^{18}O$ stack (Lisiecki and Raymo, 2005). (b) MAR_{opal} and MAR_{TOC} at Site U1524A. (c) Benthic foraminiferal $\delta^{13}C$ differences between ODP Site 704/1090 and DSDP Site 607, and benthic foraminiferal $\delta^{13}C$ at ODP Site 704/1090 (Hodell and Venz, 2006). (d) MAR_{Fe} at ODP Site 1090 (Martínez-Garcia et al., 2011). (e) Sea ice diatom content in core AND-1B (McKay et al., 2012). (f) Average summer insolation at 75°S (Laskar et al., 2004). (g) Atmospheric pCO_2 based on model simulations (Stap et al., 2016, black), planktonic foraminiferal $\delta^{11}B$ (Bartoli et al., 2011, blue), and planktonic foraminiferal B/Ca (Tripati et al., 2009, green). The vertical dashed lines mark the three stages of the evolution of productivity, and gray shading indicates the oNHG.

period, but according to the available records, it is unlikely that there was a gradual increase in sea ice intensity (Figure 3e; McKay et al., 2012), suggesting that light conditions were not the main factor controlling productivity. In addition, at ~2.7 Ma (oNHG), productivity did not change significantly, yet its potential controls such as deep ocean ventilation and eolian dust changed significantly (Figure 3a, 3c, 3d), suggesting that productivity did not generate the impact on or response to the oNHG.

The productivity at Site U1524A remained roughly stable during 2.6–2.4 Ma (Figure 3b). During this period, deep ocean ventilation fluctuated frequently but also remained generally stable (Figure 3c). However, the eolian dust input slowly decreased, followed by a rapid increase (Figure 3d). Although insolation remained stable during this period, the lack of sea ice intensity records made it challenging to assess the impact of light conditions on productivity (Figure 3e, 3f). Based on the relationships between productivity and potential controls during 2.6–2.4 Ma, it seems that deep ocean ventilation still controlled the productivity during this period.

5.2.2 Factors controlling the long-term trend of productivity

The productivity at Site U1524A exhibited a long-term decreasing trend during 3.3–2.4 Ma (Figure 3b). The deep ocean ventilation also showed a long-term weakening trend during this time interval (Figure 3c). Due to the lack of continuous sea ice intensity records for 3.3–2.4 Ma, we are currently unable to discuss the potential influence from light conditions. If light conditions controlled the long-term trend of productivity, then sea ice intensity should have show a long-term increasing trend. However, according to the existing sea ice intensity data during 3.3–2.4 Ma (Figure 3e), it is unlikely to show a long-term increasing trend in any case. In addition, the eolian dust input remained stable before the oNHG and increased significantly after the oNHG (Figure 3d). Based on the above comparisons between records, it is concluded that deep ocean ventilation controlled the long-term evolution of AZ productivity during 3.3–2.4 Ma. In summary, deep ocean ventilation, rather than eolian dust input or light, controlled productivity in the SO both on orbital timescales and long-term trend. Specifically, enhanced ocean ventilation upwells more deep nutrients to the surface, thus increasing productivity.

5.3 Productivity variations linked to atmospheric pCO_2 cycles

Productivity, deep ocean ventilation, and temperature in the SO reveal significant covariance with atmospheric pCO_2 on orbital scales. In this study, we test the applicability of the above mechanisms to timescales longer than glacial-interglacial cycles by comparing NHG Ross Sea productivity with atmospheric pCO_2. The Ross Sea productivity covaried with the modeled atmospheric pCO_2 (Stap et al., 2016) (Figure 3g) during 3.3–3.0 Ma, exhibiting that increased productivity corresponds to elevated atmospheric pCO_2. According to the "respired CO_2" hypothesis (Jaccard et al., 2009), if productivity controls the uptake of CO_2 at the sea surface, then increased productivity should correspond to decreased atmospheric pCO_2, i.e., productivity should be inversely related to atmospheric pCO_2. Moreover, there was no significant inverse phase relationship between productivity and atmospheric pCO_2 during either 3.0–2.6 Ma or 2.6–2.4 Ma (Figure 3b, 3g). In particular, at the oNHG, atmospheric pCO_2 decreased significantly, while productivity remained relatively constant. These results suggest that the evolution of productivity in the AZ was not the primary cause of variations in atmospheric pCO_2 on orbital timescales. There was a long-term decrease in productivity during 3.3–2.4 Ma, yet neither the low-resolution atmospheric pCO_2 reconstruction record nor the high-resolution atmospheric pCO_2 modeling record demonstrated a long-term increasing trend (Figure 3b, 3g). Therefore, the long-term evolution of productivity in the AZ is also not the main cause of atmospheric pCO_2 variations.

These findings provide insights into the role of the SO in atmospheric pCO_2 variation and the regulation of the NHG through the "atmospheric bridge". First, we suggest that productivity in the AZ is not the primary factor controlling atmospheric pCO_2, which is consistent with the mechanism of atmospheric pCO_2 during glacial-interglacial cycles (Jaccard et al., 2013; Martínez-García et al., 2014), i.e., the AZ contributes to atmospheric pCO_2 glacial-interglacial cycles through deep ocean ventilation rather than surface productivity. Next, a comprehensive reconstruction of deep ocean ventilation in the Ross Sea using sediment grain size, Sr-Nd isotopes, and redox elements at Site U1524A should be performed to assess the impact of the deep ventilation on the evolution of atmospheric pCO_2 in the AZ. Furthermore, similar studies should be extended to the SAZ of the SO.

6. Conclusion

Based on the biogenic components at IODP Expedition 374 Site U1524A, this study discussed the characteristics and controls of productivity in the AZ and its link to atmospheric pCO_2. During 3.3–2.4 Ma, the productivity exhibited a three-stage evolution with a long-term decreasing trend, which is dominated by changes in deep ocean ventilation. Sea ice intensity may have played a role in changes of productivity during 3.3–3.0 Ma, while eolian dust inputs had little effect at the whole study intervals. AZ productivity was not the major factor controlling the atmospheric pCO_2 decrease

during the NHG. Further studies should focus on the potential influences of deep ocean ventilation on atmospheric pCO_2 in the AZ, and similar studies should also be extended to the sea area in the SAZ.

Acknowledgements *We would like to express our gratitude to the scientists, technicians and crew of IODP Expedition 374 for their efforts in drilling sediment cores. We also thank the two anonymous peer reviewers for their constructive comments on this manuscript. This work was supported by the National Natural Science Foundation of China (Grant Nos. 42076232 & 42006075), the Impact and Response of Antarctic Seas to Climate Change Program (Grant No. IRASCC2020-2022-No.01-03-02), and the Taishan Scholars Projects Funding (Grant Nos. TS20190963 & TSQN202211265).*

Conflict of interest The authors declare that there are no conflicts of interest.

References

Arrigo K R, van Dijken G L. 2003. Phytoplankton dynamics within 37 Antarctic coastal polynya systems. J Geophys Res, 108: 2002JC001739
Arrigo K R, van Dijken G L, Bushinsky S. 2008. Primary production in the Southern Ocean, 1997–2006. J Geophys Res, 113: 2007JC004551
Ballantyne A P, Axford Y, Miller G H, Otto-Bliesner B L, Rosenbloom N, White J W C. 2013. The amplification of Arctic terrestrial surface temperatures by reduced sea-ice extent during the Pliocene. Palaeogeogr Palaeoclimatol Palaeoecol, 386: 59–67
Ballantyne A P, Greenwood D R, Sinninghe Damsté J S, Csank A Z, Eberle J J, Rybczynski N. 2010. Significantly warmer Arctic surface temperatures during the Pliocene indicated by multiple independent proxies. Geology, 38: 603–606
Bartoli G, Hönisch B, Zeebe R E. 2011. Atmospheric CO_2 decline during the Pliocene intensification of Northern Hemisphere glaciations. Paleoceanography, 26: 2010PA002055
Basak C, Pahnke K, Frank M, Lamy F, Gersonde R. 2015. Neodymium isotopic characterization of Ross Sea Bottom Water and its advection through the southern South Pacific. Earth Planet Sci Lett, 419: 211–221
Blake-Mizen K, Hatfield R G, Stoner J S, Carlson A E, Xuan C, Walczak M, Lawrence K T, Channell J E T, Bailey I. 2019. Southern Greenland glaciation and Western Boundary Undercurrent evolution recorded on Eirik Drift during the late Pliocene intensification of Northern Hemisphere glaciation. Quat Sci Rev, 209: 40–51
Boyd P W. 2002. Environmental factors controlling phytoplankton processes in the southern ocean. J Phycol, 38: 844–861
Brierley C M, Fedorov A V, Liu Z, Herbert T D, Lawrence K T, LaRiviere J P. 2009. Greatly expanded tropical warm pool and weakened Hadley circulation in the early Pliocene. Science, 323: 1714–1718
Cane M A, Molnar P. 2001. Closing of the Indonesian seaway as a precursor to east African aridification around 3–4 million years ago. Nature, 411: 157–162
Clark P U, Alley R B, Pollard D. 1999. Northern hemisphere ice-sheet influences on global climate change. Science, 286: 1104–1111
Comiso J C, McClain C R, Sullivan C W, Ryan J P, Leonard C L. 1993. Coastal zone color scanner pigment concentrations in the Southern Ocean and relationships to geophysical surface features. J Geophys Res, 98: 2419–2451
DeConto R M, Pollard D, Wilson P A, Pälike H, Lear C H, Pagani M. 2008. Thresholds for Cenozoic bipolar glaciation. Nature, 455: 652–656
DeMaster D J. 1981. The supply and accumulation of silica in the marine environment. Geochim Cosmochim Acta, 45: 1715–1732
Fetterer F, Knowles K, Meier W N, Savoie M, Windnagel A K. 2017. Sea Ice Index. Version 3. NSIDC: National Snow and Ice Data Center, Boulder, Colorado USA
Fischer H, Schmitt J, Lüthi D, Stocker T F, Tschumi T, Parekh P, Joos F, Köhler P, Völker C, Gersonde R, Barbante C, Le Floch M, Raynaud D, Wolff E. 2010. The role of Southern Ocean processes in orbital and millennial CO_2 variations—A synthesis. Quat Sci Rev, 29: 193–205
Gordon A L, Zambianchi E, Orsi A, Visbeck M, Giulivi C F, Whitworth Iii T, Spezie G. 2004. Energetic plumes over the western Ross Sea continental slope. Geophys Res Lett, 31: 2004GL020785
Hall A. 2004. The role of surface albedo feedback in climate. J Clim, 17: 1550–1568
Haug G H, Sigman D M, Tiedemann R, Pedersen T F, Sarnthein M. 1999. Onset of permanent stratification in the subarctic Pacific Ocean. Nature, 401: 779–782
Haywood A M, Valdes P J. 2004. Modelling Pliocene warmth: contribution of atmosphere, oceans and cryosphere. Earth Planet Sci Lett, 218: 363–377
Hillenbrand C D, Cortese G. 2006. Polar stratification: A critical view from the Southern Ocean. Palaeogeogr Palaeoclimatol Palaeoecol, 242: 240–252
Hodell D A, Venz K A. 1992. Toward A High-Resolution Stable Isotopic Record of the Southern Ocean during the Pliocen-Pleistocene (4.8 to 0.8 Ma). The Antarctic Paleoenvironment: A Perspective on Global Change: Part One, 56: 265–310
Hodell D A, Venz K A. 2006. Late Neogene history of deepwater ventilation in the Southern Ocean. Geochem Geophys Geosyst, 7: 2005GC001211
Jaccard S L, Galbraith E D, Sigman D M, Haug G H, Francois R, Pedersen T F, Dulski P, Thierstein H R. 2009. Subarctic Pacific evidence for a glacial deepening of the oceanic respired carbon pool. Earth Planet Sci Lett, 277: 156–165
Jaccard S L, Hayes C T, Martínez-García A, Hodell D A, Anderson R F, Sigman D M, Haug G H. 2013. Two modes of change in Southern Ocean productivity over the past million years. Science, 339: 1419–1423
Jaramillo C, Montes C, Cardona A, Silvestro D, Antonelli A, Bacon C D. 2017. Comment (1) on "Formation of the Isthmus of Panama" by O'Dea *et al*. Sci Adv, 3: e1602321
Khatiwala S, Primeau F, Hall T. 2009. Reconstruction of the history of anthropogenic CO_2 concentrations in the ocean. Nature, 462: 346–349
Laskar J, Robutel P, Joutel F, Gastineau M, Correia A C M, Levrard B. 2004. A long-term numerical solution for the insolation quantities of the Earth. Astron Astrophys, 428: 261–285
Lisiecki L E, Raymo M E. 2005. A Pliocene-Pleistocene stack of 57 globally distributed benthic $\delta^{18}O$ records. Paleoceanography, 20: 2004PA001071
Liu S, Zhou C, Wang Z. 2016. Comparative analysis of changes in sea ice extent in Ross Sea and Prydz Bay (in Chinese). Chin J Polar Res. 28: 228–234
Lüthi D, Le Floch M, Bereiter B, Blunier T, Barnola J M, Siegenthaler U, Raynaud D, Jouzel J, Fischer H, Kawamura K, Stocker T F. 2008. High-resolution carbon dioxide concentration record 650,000–800,000 years before present. Nature, 453: 379–382
Martínez-Botí M A, Foster G L, Chalk T B, Rohling E J, Sexton P F, Lunt D J, Pancost R D, Badger M P S, Schmidt D N. 2015. Addendum: Plio-Pleistocene climate sensitivity evaluated using high-resolution CO_2 records. Nature, 526: 458
Martínez-Garcia A, Rosell-Melé A, Jaccard S L, Geibert W, Sigman D M, Haug G H. 2011. Southern Ocean dust-climate coupling over the past four million years. Nature, 476: 312–315
Martínez-García A, Sigman D M, Ren H, Anderson R F, Straub M, Hodell D A, Jaccard S L, Eglinton T I, Haug G H. 2014. Iron fertilization of the subantarctic ocean during the last ice age. Science, 343: 1347–1350
Massom R A, Stammerjohn S E. 2010. Antarctic sea ice change and variability—Physical and ecological implications. Polar Sci, 4: 149–186
McKay R, Naish T, Carter L, Riesselman C, Dunbar R, Sjunneskog C, Winter D, Sangiorgi F, Warren C, Pagani M, Schouten S, Willmott V, Levy R, DeConto R, Powell R D. 2012. Antarctic and Southern Ocean influences on Late Pliocene global cooling. Proc Natl Acad Sci USA, 109: 6423–6428

McKay R, De Santis L, Kulhanek D K, Ash J L, Beny F, Browne I M, Cortese G, Cordeiro De Sousa I M, Dodd J P, Esper O M, Gales J A, Harwood D M, Ishino S, Keisling B A, Kim S, Kim S, Laberg J S, Leckie R M, Müller J, Patterson M O, Romans B W, Romero O E, Sangiorgi F, Seki O, Shevenell A E, Singh S M, Sugisaki S T, Van De Flierdt T, Van Peer T E, Xiao W, Xiong Z. 2019. Ross Sea West Antarctic ice sheet history. Proceedings of the International Ocean Discovery Program 374, doi: 10.14379/iodp.374.106.2019

Moore J K, Abbott M R. 2000. Phytoplankton chlorophyll distributions and primary production in the Southern Ocean. J Geophys Res, 105: 28709–28722

Mortlock R A, Froelich P N. 1989. A simple method for the rapid determination of biogenic opal in pelagic marine sediments. Deep Sea Res Part A Oceanogr Res Papers, 36: 1415–1426

Mudelsee M, Raymo M E. 2005. Slow dynamics of the Northern Hemisphere glaciation. Paleoceanography, 20: 2005PA001153

Müller P J, Schneider R. 1993. An automated leaching method for the determination of opal in sediments and particulate matter. Deep Sea Res Part I-Oceanogr Res Papers, 40: 425–444

Naish T, Powell R, Levy R, Wilson G, Scherer R, Talarico F, Krissek L, Niessen F, Pompilio M, Wilson T, Carter L, DeConto R, Huybers P, McKay R, Pollard D, Ross J, Winter D, Barrett P, Browne G, Cody R, Cowan E, Crampton J, Dunbar G, Dunbar N, Florindo F, Gebhardt C, Graham I, Hannah M, Hansaraj D, Harwood D, Helling D, Henrys S, Hinnov L, Kuhn G, Kyle P, Läufer A, Maffioli P, Magens D, Mandernack K, McIntosh W, Millan C, Morin R, Ohneiser C, Paulsen T, Persico D, Raine I, Reed J, Riesselman C, Sagnotti L, Schmitt D, Sjunneskog C, Strong P, Taviani M, Vogel S, Wilch T, Williams T. 2009. Obliquity-paced Pliocene West Antarctic ice sheet oscillations. Nature, 458: 322–328

O'Dea A, Lessios H A, Coates A G, Eytan R I, Restrepo-Moreno S A, Cione A L, Collins L S, de Queiroz A, Farris D W, Norris R D, Stallard R F, Woodburne M O, Aguilera O, Aubry M P, Berggren W A, Budd A F, Cozzuol M A, Coppard S E, Duque-Caro H, Finnegan S, Gasparini G M, Grossman E L, Johnson K G, Keigwin L D, Knowlton N, Leigh E G, Leonard-Pingel J S, Marko P B, Pyenson N D, Rachello-Dolmen P G, Soibelzon E, Soibelzon L, Todd J A, Vermeij G J, Jackson J B C. 2016. Formation of the isthmus of Panama. Sci Adv, 2: e1600883

Orsi A H, Smethie Jr. W M, Bullister J L. 2002. On the total input of Antarctic waters to the deep ocean: A preliminary estimate from chlorofluorocarbon measurements. J Geophys Res, 107: 3122

Pondaven P, Ragueneau O, Tréguer P, Hauvespre A, Dezileau L, Reyss J L. 2000. Resolving the 'opal paradox' in the Southern Ocean. Nature, 405: 168–172

Raymo M E. 1994. The initiation of northern hemisphere glaciation. Annu Rev Earth Planet Sci, 22: 353–383

Rea D K, Janecek T R. 1981. Late cretaceous history of eolian deposition in the mid-pacific mountains, central North Pacific Ocean. Palaeogeogr Palaeoclimatol Palaeoecol, 36: 55–67

Riesselman C R, Dunbar R B. 2013. Diatom evidence for the onset of Pliocene cooling from AND-1B, McMurdo Sound, Antarctica. Palaeogeogr Palaeoclimatol Palaeoecol, 369: 136–153

Ruddiman W F, Raymo M, McIntyre A. 1986. Matuyama 41,000-year cycles: North Atlantic Ocean and northern hemisphere ice sheets. Earth Planet Sci Lett, 80: 117–129

Salzmann U, Haywood A M, Lunt D J, Valdes P J, Hill D J. 2008. A new global biome reconstruction and data-model comparison for the Middle Pliocene. Glob Ecol Biogeogr, 17: 432–447

Seki O, Foster G L, Schmidt D N, Mackensen A, Kawamura K, Pancost R D. 2010. Alkenone and boron-based Pliocene pCO_2 records. Earth Planet Sci Lett, 292: 201–211

Sigman D M, Jaccard S L, Haug G H. 2004. Polar ocean stratification in a cold climate. Nature, 428: 59–63

Smith W, Sedwick P, Arrigo K, Ainley D, Orsi A. 2012. The Ross Sea in a sea of change. Oceanography, 25: 90–103

Stap L B, de Boer B, Ziegler M, Bintanja R, Lourens L J, van de Wal R S W. 2016. CO_2 over the past 5 million years: Continuous simulation and new δ^{11}B-based proxy data. Earth Planet Sci Lett, 439: 1–10

Thompson A F, Stewart A L, Spence P, Heywood K J. 2018. The Antarctic slope current in a changing climate. Rev Geophys, 56: 741–770

Trathan P N, Brandon M A, Murphy E J, Thorpe S E. 2000. Transport and structure within the Antarctic Circumpolar Current to the north of south Georgia. Geophys Res Lett, 27: 1727–1730

Tripati A K, Roberts C D, Eagle R A. 2009. Coupling of CO_2 and ice sheet stability over major climate transitions of the last 20 million years. Science, 326: 1394–1397

Venz K A, Hodell D A. 2002. New evidence for changes in Plio-Pleistocene deep water circulation from Southern Ocean ODP Leg 177 Site 1090. Palaeogeogr Palaeoclimatol Palaeoecol, 182: 197–220

Watson A J, Garabato A C N. 2006. The role of Southern Ocean mixing and upwelling in glacial-interglacial atmospheric CO_2 change. Tellus B-Chem Phys Meteor, 58: 73–87

Watson A J, Vallis G K, Nikurashin M. 2015. Southern Ocean buoyancy forcing of ocean ventilation and glacial atmospheric CO_2. Nat Geosci, 8: 861–864

Willeit M, Ganopolski A, Calov R, Robinson A, Maslin M. 2015. The role of CO_2 decline for the onset of Northern Hemisphere glaciation. Quat Sci Rev, 119: 22–34

Wright J D, Miller K G. 1996. Control of north atlantic deep water circulation by the Greenland-scotland ridge. Paleoceanography, 11: 157–170

Woodard S C, Rosenthal Y, Miller K G, Wright J D, Chiu B K, Lawrence K T. 2014. Antarctic role in Northern Hemisphere glaciation. Science, 346: 847–851

(Editorial handling: Shouye YANG)